CHEMISTRY
A EUROPEAN JOURNAL

DOI: 10.1002/chem.200701163

Tuning the Charge Distribution and Photoswitchable Properties of Cobalt–Dioxolene Complexes by Using Molecular Techniques

Alessandra Beni,[a] Andrea Dei,*[a] Serena Laschi,[b] Mario Rizzitano,[a] and Lorenzo Sorace[a]

Abstract: A series of cobalt complexes $[Co(Me_ntpa)(diox)]PF_6 \cdot sol$ (diox = 3,5-di-*tert*-butyl-1,2-dioxolene; sol = ethanol, toluene; tpa = tris(2-pyridylmethyl)amine) were prepared by using tripod-like Me_ntpa ($n = 0$, 1, 2, 3), derived from tpa by successive introduction of methyl groups into the 6-position of the pyridine moieties, as an ancillary ligand. The steric hindrance induced by this substitution modulates the redox properties of the metal acceptor, thus determining the charge distribution of the metal–dioxolene moiety at room temperature. All of these complexes were characterised by using diffractometric studies, electronic spectroscopic analysis, and magnetic susceptibility measurements. In the solid state, the $[Co(Me_ntpa)(diox)]^+$ ions ($n = 0$, 1) can be described as diamagnetic cobalt(III)–catecholato derivatives, whereas a cobalt(II)–semiquinonato description seems appropriate for the paramagnetic $[Co(Me_3tpa)(diox)]^+$ complex. The complex $[Co(Me_2tpa)(diox)]PF_6 \cdot C_2H_5OH$ undergoes entropy-driven valence tautomeric interconversion at room temperature. Optically induced valence tautomerism was observed by irradiation of $[Co(Me_ntpa)(diox)]PF_6$ complexes ($n = 0$, 1, 2) at cryogenic temperatures. The different relaxation kinetics of the photoinduced metastable phases are related to the respective free-energy changes of the interconversion, as estimated by cyclic voltammetric experiments at room temperature, and to the different lattice interactions, as supported by structural data. These results show the importance of molecular techniques for controlling the relaxation properties of photoinduced metastable species. At the same time, this behaviour strongly suggests that this paradigm exhibits intrinsic limits because of the less controllable factors that affect the process.

Keywords: cobalt · magnetic properties · photochemistry · semiquinones · valence isomerization

Introduction

Photoinduced electron transfer may be exploited in many potential applications that deal with the conversion of quantum photon energy into chemical potential energy. In particular, the charge separation of the chromophore, which is set up after the absorption of the photon, may in turn be used either as a memory bit of information or for triggering the primary reaction that establishes an useful potential gradient.[1–3] As an example, we can think of transmembrane potential differences in biological systems[4,5] and of the electric potential associated with electron–hole pairs in which the chromophore is anchored to a semiconductor material.[6–8] The practical application of this phototriggered event is, however, intrinsically related to the whole duration of the dynamic processes involved in the relaxation of the perturbed chromophore.

The phototriggered processes occur with a well-defined mechanism that couples the electronic ground state of the chromophore with the electronic excited states. The relaxation of the excited state into the lower-energy states involves several mechanisms, such as internal conversion, intersystem crossing, vibrational relaxation, and so forth. Quantum mechanically, if the decay process occurs through intersystem crossing, we expect to have an activated, radiationless transition between different electronic states of the chromophore. If the wave functions Ψ_i and Ψ_j describe the initial and the

[a] Dr. A. Beni, Prof. A. Dei, M. Rizzitano, Dr. L. Sorace
LAMM, INSTM Research Unit and Dipartimento di Chimica
Università di Firenze, Via della Lastruccia 3
50019 Sesto Fiorentino (Firenze) (Italy)
Fax: (+39) 0554573372
E-mail: andrea.dei@unifi.it

[b] Dr. S. Laschi
Dipartimento di Chimica Università di Firenze
Via della Lastruccia 3
50019 Sesto Fiorentino (Firenze) (Italy)

Supporting information for this article is available on the WWW under http://www.chemeurj.org/ or from the author.

final electronic states, respectively, the rate constant k of the process is given by the following relationship:[9]

$$k = (4\pi^2/h)|V|^2G \quad (1)$$

where V is the electronic coupling matrix element $<\Psi_i|\boldsymbol{H}|\Psi_j>$ ($\boldsymbol{H}$ is the total electronic Hamiltonian) that depends on the overlap between the wave functions Ψ_i and Ψ_j, and G is the thermally averaged nuclear Franck–Condon vibrational overlap factor. As a general expectation, this value will be large if the two wave functions have the same spin multiplicity, but will be small when their character is different. To obtain long-lived photoinduced charge separation, chromophores characterised by low-lying excited states with a different spin multiplicity than the ground state one are then actively investigated. In this way, the spin-forbidden character of the transition may slow down the relaxation from the excited state to the ground state. In these cases, one attractive feature of the photoinduced phenomenon lies in the possibility of observing a long-lived change in the magnetic properties of the sample. Within this framework, therefore, the photocontrol of the magnetic properties of molecular systems is a key factor in the development of systems with potential technological applications such as optical switching devices.[10–14] However, the incomplete comprehension of the factors that affect the photochromic behaviour of many compounds has up to now precluded the possibility of designing new systems based on a well-defined strategy.

Studies concerning the light-induced excited spin-state trapping (LIESST) effect observed for iron(II) spin crossover derivatives suggest that the lifetime of the photoinduced metastable species is strictly related to the existence of two low-lying electronic states of different spin multiplicities that are close in energy and are characterized by large differences in molecular geometry.[15–19] Similar arguments have been used to explain the observation that some cobalt–catecholato derivatives exhibit a photoinduced valence-tautomeric (VT) interconversion[10–12,20–38]

$$\text{ls-}[Co^{III}(L)(Cat)]^+ \overset{T,\,h\nu}{\rightleftharpoons} \text{hs-}[Co^{II}(L)(SQ)]^+ \quad (2)$$

where L is an ancillary ligand, Cat is the catecholato ligand, and SQ is the semiquinonato ligand. The process is characterised by a large variation in the magnetic properties, since the cobalt(III)–catecholato complex is diamagnetic, the cobalt(II) ion is in the high-spin (hs) configuration, and the semiquinonato ligand is a radical species. Also in this case, the large lifetimes that often characterise the photoinduced metastable hs species can be justified in terms of geometric differences between the two redox isomers and free-energy changes associated with Equation (2). Indeed, the above interconversion is accompanied by a significant change in Co–O bond lengths (about 0.18–0.21 Å), as expected on the basis of the change in the population of the σ* orbitals of the metal ion. Therefore, in the usual representation of the Gibbs potential energy (Figure 1), it is expected that a significant horizontal displacement exists between the two species involved in the electron-transfer process.

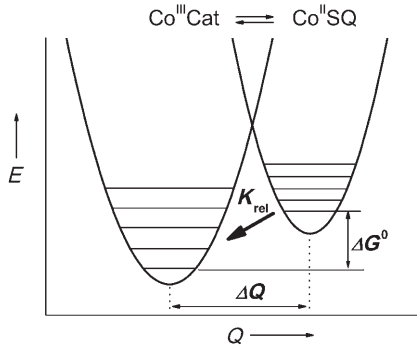

Figure 1. Potential-energy wells for the valence-tautomeric interconversion process.

For spin-crossover complexes, the relaxation kinetics of photoinduced metastable phases have been successfully interpreted by Hauser and co-workers[17,40] by working out a nonadiabatic multiphonon relaxation model on the basis of the theory developed by Jortner and co-workers for radiationless relaxation decay.[41] Following this model, it has been suggested[22,29] that the relaxation rate of the photoinduced metastable species in VT cobalt–dioxolene complexes decreases with increasing changes in the Co–O bond lengths and wit decreasing the energy gap between the metastable and ground states $\Delta G°$ (see Figure 1).

In this sense, the key parameters that are expected to play a determining role in the relaxation kinetics are the value of the electronic coupling V, the change in geometry, and the energy gap. In analogy with the spin-crossover complexes, the two wave functions of the donor and acceptor states are orthogonal, and electronic coupling is, therefore, allowed only by spin–orbit coupling interactions. It can be expected that along a series of similar complexes this quantity should be small and have similar absolute values. As far as the geometric changes are concerned, it has to be considered that the electronic delocalization within the metallacycle chelate ring in the 3d-metal/dioxolene complex is low.[21–25] Therefore, along the same series of cobalt–dioxolene complexes the geometric difference between cobalt(III)–catecholato species and the corresponding cobalt(II)–semiquinonato species are also expected to be similar. It must be concluded that the only way to modulate the rate of the electronic ground-state recovery is by controlling the extent of the energy gap $\Delta G°$. This control cannot be achieved with spin-crossover complexes, but we suggest herein that it may be possible in the case of cobalt–dioxolene complexes on the basis of the following considerations.

As mentioned above, it can be reasonably assumed that the energy of the electronic levels of the coordinated dioxolenes should depend only on their ionic charge density, while being roughly independent from the electronic properties of the 3d-metal ions. In practice, this assumption means that once the free-energy changes involved in the ligand-

centred redox processes $[M^{II}(L)SQ]+e^- \rightarrow [M^{II}(L)(Cat)]$ have been corrected for the different ligand-field stabilization energies they should be similar for divalent 3d-metal ions. Therefore, the free-energy change associated with Equation (2) can be calculated as the difference between the redox potential of the above-mentioned ligand-centred redox process and the redox potential of the metal-centred $[M^{III}(L)(Cat)]+e^- \rightarrow [M^{II}(L)(Cat)]$ process (Scheme 1).

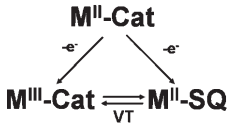

Scheme 1. Thermodynamical processes involved in VT equilibrium.

The ΔS changes associated with Equation (2) are expected to be similar within a series of related [Co(L)diox] complexes because of the isoelectric character of the reaction and the similar electronic and vibrational entropy contributions. Therefore, the observed free-energy changes at room temperature should parallel the free-energy (enthalpy) pattern at cryogenic temperatures. It should, however, be stressed that nothing can be predicted about the role of the intermolecular interactions in the solid state that affect both the activation energy and the free-energy difference of the electron-transfer process.

The approach described herein was used some years ago for analysing the energies of the ligand-to-metal charge-transfer (LMCT) transitions in some iron(III)–catecholato complexes[42] and for planning the synthesis of a dioxolene adduct of a cobalt–tetraaza macrocycle acceptor, in order to obtain a compound that undergoes valence-tautomeric interconversion.[43] Herein, we will show how the photoswitchable properties of a family of 1:1 cobalt–dioxolene complexes can be explained following this simple predictive scheme. However, in the following pages we will also show the intrinsic limitations of this approach, based on the assessment of the free energy of the process in solution.

We synthesised a series of cobalt compounds with the general formula $[Co(Me_ntpa)(diox)]PF_6$ (diox = 3,5-di-*tert*-butyl-1,2-dioxolene (Dbdiox) and tetrachloro-*o*-dioxolene), which had tripod-like Me_ntpa ($n = 0$, 1, 2, 3), derived from tris(2-pyridylmethyl)amine (tpa) by successive introduction of methyl groups into the 6-position of the pyridine moieties, as an ancillary ligand. The steric hindrance induced by this substitution is expected to modulate the redox properties of the metal acceptor,[44] thus determining the charge distribution of the metal–dioxolene moiety at room temperature. The observed different charge distributions of these complexes (i.e., Co^{III}–Cat or Co^{II}–SQ) fits well with those expected on the basis of the free-energy changes for Equation (2) extrapolated by cyclic-voltammetric studies of these complexes, their tetrachlorocatecholato derivatives, and the nickel(II) analogues. This approach also allows the prediction of the entropy-driven VT interconversion for one of the isolated compounds. The observed kinetics parameters relative to the relaxation of the photoinduced metastable phases will be finally discussed by taking into account the above-mentioned considerations. The results of the characterisation of compounds containing other dioxolene ligands will be reported later. A preliminary account of some of the experimental results reported herein has recently been published.[45]

Results

Synthesis: The four Me_ntpa ligands were prepared by using a general one-step procedure, according to the recently reported preparation of tpa.[46] Treatment of pyridine-2-carboxyaldheyde with 2-aminomethylpyridine (mol/mol = 2:1) in dichloromethane in the presence of triacetoxyborohydride yielded the tpa ligand in 89% yield. We extended this procedure by using the appropriate 6-methyl analogues, thus obtaining the Me_ntpa ligands in similar yields (80–90%; Scheme 2).

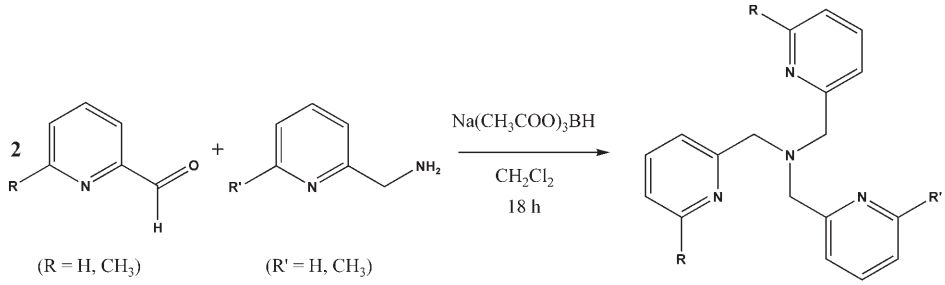

Scheme 2. Preparation of Me_ntpa ligands.

Solid compounds $[Co(Me_ntpa)(DBdiox)]PF_6 \cdot x\,solv$ (DBdiox = DBCat, DBSQ; solv = water, ethanol, toluene; tpa = **1**, Me_1tpa = **2**, Me_2tpa = **3**, Me_3tpa = **4**) were obtained in a one-step reaction by mixing equimolar amounts of cobalt(II) salts, the Me_ntpa ligand, and catechol in the presence of triethylamine. Although not always necessary, all these manipulations were carried out in an inert atmosphere. The solutions containing the $[Co^{II}(Me_ntpa)(DBCat)]$ complexes were oxidized with dioxygen and the resulting products isolated as PF_6 salts. The tetrachlorocatecholato (TCCat) analogues were obtained either as $[Co^{II}(Me_ntpa)(TCCat)]$ or $[Co^{III}(Me_ntpa)(TCCat)]PF_6$, and their properties will be described elsewhere. The $[Ni^{II}(Me_ntpa)(DBSQ)]PF_6$ complexes were obtained directly in air.

Electronic spectra: The electronic spectra of solutions of **1**–**4** in dichloromethane are shown in Figure 2, and the spectral parameters are reported in the Experimental Section. The spectral features of both **1** and **2** are consistent with the exis-

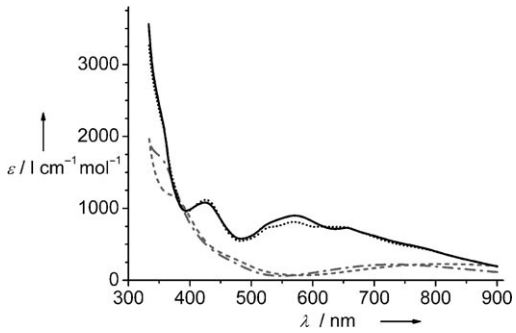

Figure 2. Electronic spectra of **1** (grey, dash-dotted line), **2** (grey, dashed line), **3** (black, continuous line), and **4** (black, dotted line).

tence of cobalt(III)–catecholato chromophores.[47] Indeed, the broad bands in the red region of the spectrum are consistent with symmetry-forbidden LMCT transitions, whereas the transitions at 23200 and 21550 cm^{-1} (430 and 465 nm, respectively) in the spectra of **1** and **2**, respectively, can be assigned to the d–d transitions ($^1A_{1g} \rightarrow {}^1T_{1g}$ in O_h)[48] typical for six-coordinate cobalt(III) chromophores. The pattern of absorption bands observed in the spectra of **3** and **4** suggests the existence of six-coordinate cobalt(II)–semiquinonato chromophores.[49] The broad transitions centred at 12500 cm^{-1} (800 nm) can be assigned to internal ligand transitions, whereas the pattern of bands at 15000–19000 cm^{-1} (665–525 nm) are attributed to charge-transfer (CT) transitions involving the d orbitals of the metal ion and the singly occupied π* orbital of the ligand.

The different charge distributions observed in these complexes are due to the different donor properties of the tripod-like ligands towards the metal ions. It is apparent that the steric hindrance induced by the *ortho*-methyl groups induces stabilisation of the cobalt(II) ion with respect to the cobalt(III) ion. The same effect probably occurs in the case of nickel(II) complexes, but the redox potential of the Ni^{III}/Ni^{II} couple, higher than the Co^{III}/Co^{II} couple, remains largely above the redox potential of the SQ/Cat couple so that all the nickel complexes show the nickel(II)–semiquinonato charge distribution. Although not discussed herein, the spectra of the cobalt derivative of the tetrachlorocatechol are all consistent with the presence of cobalt(III)–catecholato chromophores, with the exception of the Me_3tpa complex, which undergoes valence-tautomeric interconversion in solution at room temperature.

Electrochemistry: Our main objective was the calculation of the free-energy difference between the two electronic isomers Co^{III}–Cat and Co^{II}–SQ for any DBCat complex of the different $[Co(Me_n tpa)]^{3+}$ acceptors. As mentioned above, the problem reduces to the analysis of the thermochemical cycle depicted in Scheme 1. It is rather clear that the energy difference between the electronic isomers can be calculated through the difference between the energies involved in the redox processes Co^{III}–Cat/Co^{II}–Cat and Co^{II}–SQ/Co^{II}–Cat, nevertheless only the process requiring the lowest energy will be experimentally detectable. Thus, to evaluate the free-energy changes in the thermochemical cycle, we have determined the free-energy changes of the equilibria shown in Equations (3) and (4) by cyclic-voltammetric experiments at 25 °C (Fc^+ = ferrocenium, Fc = ferrocene):

$$[Co^{II}(Me_n tpa)(TCCat)] + Fc^+ \rightarrow [Co^{III}(Me_n tpa)(TCCat)]^+ + Fc \quad (3)$$

$$[Ni(Me_n tpa)(dbcat)] + Fc^+ \rightarrow [Ni(Me_n tpa)(DBSQ)]^+ + Fc \quad (4)$$

It is evident from the data reported in Table 1 that, as observed for copper complexes,[44] the introduction of each methyl group on the pyridine moiety shifts the ΔG value of

Table 1. Observed and estimated free-energy changes for the equilibria $[M(Me_n tpa)(diox)] + Fc^+ \rightarrow [M(Me_n tpa)(diox)]^+ + Fc$.[a–c]

[M(diox)]/[M(diox)]$^+$	Free-energy change [kJ mol^{-1}]			
	tpa	Metpa	Me_2tpa	Me_3tpa
$[Ni^{II}(DBCat)]/[Ni^{II}(DBSQ)]^+$	−87	−83	−84	−81
$[Co^{II}(TCCat)]/[Co^{III}(TCCat)]^+$	−90	−69	−42	−11
$[Co^{II}(DBCat)]/[Co^{II}(DBSQ)]^+$	−79[c]	−76[c]	−74	−75
$[Co^{II}(DBCat)]/[Co^{III}(DBCat)]^+$	−125	−95	−65[c]	−35[d]
$[Co^{III}(DBCat)]^+/[Co^{II}(DBSQ)]^+$	46[d]	19[d]	−9[d]	−40[e]

[a] M = Co, Ni; n = 0, 1, 2, 3; conditions: acetonitrile, 0.1 M NBu_4PF_6, 298 K. [b] From the average cathodic and anodic peak potentials in cyclic voltammograms recorded at 50 mV s^{-1} (estimated error: < 1 kJ mol^{-1}). [c] For solutions of approximately 10^{-3} M. [d] Estimated (estimated error: ± 6 kJ mol^{-1}). [e] Calculated as a difference of the free-energy changes of the redox isomers.

equilibrium (3) in solution towards the left by about 25 kJ mol^{-1}. In contrast, the changes in the ΔG values associated with equilibrium (4) are very similar to each other, with an average of $\Delta G = -83 \pm 3$ kJ mol^{-1}. This value fits well with $\Delta G = -90 \pm 3$ kJ mol^{-1}, as previously reported for $[M(CTH)(DBSQ)]^+$ complexes (M = Mn, Ni, Zn; CTH = *dl*-5,7,7,12,14,14-hexamethyl-1,4,8,11-tetraazacyclo-tetradecane).[42]

The values obtained for metal-based redox processes for TCCat derivatives and for ligand-based redox process for nickel(II) derivatives were then used to estimate the redox potential of undetectable processes for **1**–**4**. Indeed, it is only possible to measure the potential of the metal-centred redox process for complexes **1** and **2** (n = 0 and 1),

$$[Co^{II}(Me_n tpa)(DBCat)] + Fc^+ \rightarrow [Co^{III}(Me_n tpa)(DBCat)]^+ + Fc \quad (5)$$

whereas for complexes **3** and **4** (n = 2 and 3) only the ligand-centred process is observable:

$$[Co^{II}(Me_ntpa)(DBCat)] + Fc^+ \rightarrow [Co^{II}(Me_ntpa)(DBSQ)]^+ + Fc \quad (6)$$

It should be stressed that the free-energy changes associated with the metal-centred processes are significantly more positive ($\Delta\Delta G \approx 30\ kJ\,mol^{-1}$) for the TCCat ligand than the DBCat ligand.[42] This behaviour suggests that the more basic DBCat ligand is much better at stabilising the cobalt(III) ion than the TCCat ligand. On the other hand, the redox potentials of the ligand-centred processes are only slightly affected by the nature of the ancillary tripod ligand, as observed for the nickel(II) derivatives. Once we assumed that the free-energy changes associated with the metal- and ligand-centred processes approximately follow the same pattern observed for equilibria (2) and (3) in the **1–4** series, we tentatively estimated the undetectable free energy of the processes (see Table 1) and the free-energy differences for the different redox isomers. The latter quantities are $\Delta G =$ 46, 19, −9, and −40 kJ mol^{-1} for ligands **1–4**, respectively (estimated error $= \pm 6\ kJ\,mol^{-1}$).

X-ray structures: For all the four derivatives, the X-ray data collection was performed at 150 K to increase the somehow low diffracting power of the crystals obtained. Even if the final X-ray crystal structure determinations are not of excellent quality, they provide a strong enough frame to describe the different magnetic and electronic properties of the four derivatives. The crystallographic data and selected interatomic distances and angles for **1–4** are presented in Tables 2 and 3, respectively.

The four derivatives share common features: in particular for all of them, the molecular unit [Co(Me$_n$tpa)(DBdiox)] is monopositively charged, as the electric neutrality of the crystal is assured by the presence of one PF_6 unit. Furthermore, the cobalt ion is invariably six-coordinate in a *cis*-distorted pseudo-octahedral coordination, and the tripodal ligand Me$_n$tpa ($n = 0$–3) adopts a folded conformation around the metal ion, with DBdiox acting as a bidentate ligand. A representative example is reported in Figure 3 for $[Co^{III}(tpa)(DBcat)]PF_6$. The metal–donor bond lengths strongly indicate that **1–3** have the Co^{III}–Cat charge distribution at 150 K, whereas **4** has the Co^{II}–SQ one. This suggestion is confirmed by analysis of the C1−C2 and C−O bond lengths of the dioxolene ligand in the four derivatives, which gives a strong indication that **4** has the semiquinonato form and **1–3** the cathecolato form (Table 3).[23]

A peculiar feature of the singly methylated derivative is that the methyl group is equally disordered, with an occupa-

Table 2. Crystal data and details of the structure refinement for **1–4**.

	1	**2**	**3**	**4**
empirical formula	$C_{34}H_{44}CoF_6N_4O_3P$	$C_{40}H_{48}CoF_6N_4O_2P$	$C_{36.50}H_{49.50}CoF_6N_4O_{3.25}P$	$C_{42}H_{46}CoF_6N_4O_2P$
M_w	760.63	820.72	800.2	842.73
temperature [K]	153(2)	152(2)	150(2)	150(2)
wavelength [Å]	0.71073	0.71073	0.71073	0.71073
crystal system	monoclinic	monoclinic	monoclinic	monoclinic
space group	$P2_1/n$	$C2/c$	$P2_1/n$	$P2_1/n$
unit cell				
a [Å]	13.594(3)	29.891(6)	12.944(4)	11.562(2)
b [Å]	15.915(4)	16.057(2)	16.805(5)	31.902(5)
c [Å]	16.207(3)	21.583(3)	17.746(5)	24.196(4)
β [°]	90.647(16)	130.547(11)	100.17(3)	114.28(3)
volume [Å^3]	3506.2(13)	7872(2)	3799(2)	8135(2)
Z	4	8	4	8
ρ_{calcd} [mg m^{-3}]	1.441	1.385	1.399	1.363
μ [mm^{-1}]	0.607	0.545	0.565	0.529
$F(000)$	1584	3424	1674	3440
crystal size [mm^3]	0.46×0.29×0.12	0.36×0.21×0.11	0.41×0.24×0.13	0.5×0.3×0.1
θ_{max} [°]	23.45	23.01	21.97	18.86
index ranges	$-10 \le h \le 15$	$-32 \le h \le 32$	$-13 \le h \le 13$	$-10 \le h \le 10$
	$-17 \le k \le 14$	$-14 \le k \le 17$	$-17 \le k \le 17$	$-28 \le k \le 29$
	$-18 \le l \le 14$	$-23 \le l \le 22$	$-16 \le = \le 18$	$-16 \le l \le 21$
reflections collected	14064	19989	9697	27337
independent reflections	5076 (R(int) = 0.0989)	5452 (R(int) = 0.0531)	4414 (R(int) = 0.0637)	6327 (R(int) = 0.0784)
completeness to θ_{max} [%]	98.2	99.3	95	98.9
T_{max} and T_{min}	0.930 and 0.796	0.968 and 0.862	0.928 and 0.832	0.95 and 0.81
data/restr./param.	5076/0/426	5452/11/447	4414/0/466	6327/20/898
GOF on F^2	0.954	0.972	1.034	0.998
R indices ($I>2\sigma(I)$)	$R1 = 0.0780$ $wR2 = 0.1704$	$R1 = 0.0981$ $wR2 = 0.2789$	$R1 = 0.0798$ $wR2 = 0.1954$	$R1 = 0.084$ $wR2 = 0.2079$
R indices (all data)	$R1 = 0.1668$ $wR2 = 0.1997$	$R1 = 0.1532$ $wR2 = 0.3154$	$R1 = 0.1363$ $wR2 = 0.2428$	$R1 = 0.1399$ $wR2 = 0.2408$
$\Delta\rho_{max}/\Delta\rho_{min}$ [e Å^{-3}]	0.494/−0.797	1.253/−0.495	0.629/−0.553	0.948/−0.369

Table 3. Bond lengths and angles for **1**–**4**.[a].

	1	**2**	**3**	**4a**[b]	**4b**[b]
Bond lengths [Å]					
Co–O1	1.862(4)	1.857(6)	1.868(5)	2.022(7)	2.008(7)
Co–O2	1.881(5)	1.864(6)	1.880(5)	2.075(7)	2.086(7)
Co–N1	1.951(5)	1.962(8)	2.029(6)	2.267(10)	2.295(10)
Co–N2	1.925(5)	1.945(8)	2.017(6)	2.232(10)	2.212(10)
Co–N3	1.918(6)	1.932(8)	1.967(6)	2.129(10)	2.165(9)
Co–N4	1.910(6)	1.920(8)	1.934(7)	2.103(9)	2.091(9)
O1–C1	1.352(8)	1.368(10)	1.348(8)	1.282(12)	1.295(12)
O2–C2	1.384(7)	1.379(11)	1.343(9)	1.289(12)	1.304(12)
C1–C2	1.386(9)	1.379(13)	1.409(11)	1.437(14)	1.468(15)
Bond angles [°]					
O1-Co-O2	88.2(2)	88.1(3)	87.6(2)	79.6(3)	79.3(3)
O1-Co-N1	90.0(2)	89.6(3)	86.5(2)	91.9(4)	95.5(4)
O1-Co-N2	87.3(2)	90.7(3)	89.9(2)	92.0(3)	90.2(2)
O1-Co-N3	175.5(2)	177.2(3)	174.2(3)	171.9(4)	170.5(4)
O1-Co-N4	89.5(2)	90.3(3)	89.4(2)	89.1(4)	89.4(4)
O2-Co-N1	93.2(2)	95.4(3)	98.5(2)	101.4(4)	104.6(4)
O2-Co-N2	96.3(2)	95.7(3)	93.3(2)	104.3(4)	101.1(4)
O2-Co-N3	96.3(2)	94.0(3)	96.9(2)	107.9(4)	107.8(4)
O2-Co-N4	176.8(2)	178.4(3)	176.9(3)	168.6(4)	168.7(4)
N1-Co-N2	170.0(3)	168.9(3)	167.4(3)	154.3(5)	154.3(4)

[a] The same numbering scheme as that of **1** is assumed for all the derivatives, even if for specific reasons the corresponding CIF files may use a different scheme. [b] Compounds **4a** and **4b** are the two independent molecules in the unit cell of **4**.

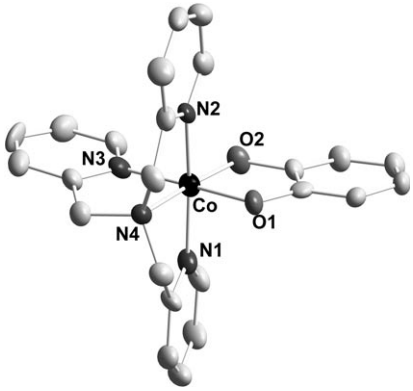

Figure 3. Diamond view of the cationic unit of **1** (ellipsoids at 40% probability level). *tert*-Butyl groups and hydrogen atoms are omitted for the sake of clarity.

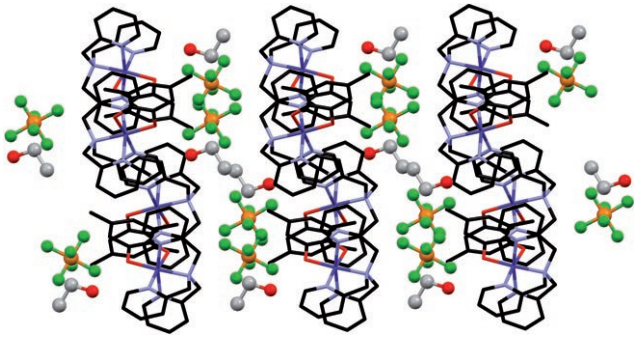

Figure 4. View of the packing of **1** along the (101) direction, thus demonstrating the alternating layers of the cationic molecules and the PF_6 and solvent molecules.

tion factor of 0.5, over the 6-position of the two pyridine rings that lie on the plane normal to the ring of the dioxolene ligand. This phenomenon reflects the possible binding of the ancillary ligand Metpa in two equally probable configurations.

The analysis of the crystal packing of the four derivatives also showed some common features. Indeed, for all of the derivatives layers containing $[Co(DBdiox)(Me_ntpa)]^+$ units are formed, which alternate with layers containing both the PF_6^- counterion and the solvent molecules (see Figure 4 for **1**).

The bidimensional layer of $[Co(DBdiox)(Me_ntpa)]^+$ molecules in **1**–**3** is characterized by an extended network of π–π stacking interactions between the pyridine rings of adjacent molecules and C–H···π interactions between the C–H bonds of a pyridine ring and both the π systems of the dioxolene and pyridine rings of the adjacent molecule (see Figure 5a). It is worth noting that the interactions are expected to decrease in the order **2** > **3** > **1**. Indeed, this order reflects that of the distances between the centroids of the interacting pyridine rings, which vary from 3.83 Å for **2** to 3.92 Å for **3** and 4.01 Å for **1**, with the average angle between the normal-to-plane and the centroid–centroid connection correspondingly being 21.7° for **2**, 33.9° for **3**, and 30.5° for **1**; the deviation from parallelism between the interacting planes is minimal for **2** and maximal for **1**.[50] As for the C–H···π interaction, the distance between the carbon atom in the 3-position of the pyridine unit and the centroid of the dioxolene ligand is 3.51 Å (average) for **2** and **3** and about 3.65 Å for **1**. On the other hand, the situation is very different for **4**, whose asymmetric unit contains two $[Co(Me_3tpa)(diox)]^+$ molecules that strongly interact through π stacking interactions between two pyridine rings (see Figure 5b). The distance between centroids is only 3.43 Å, whereas no extended interactions between adjacent dimers can be detected (the centroid–centroid distance between parallel adjacent rings is larger than 4 Å). This behaviour may be considered to be a consequence of the different charge distribution in

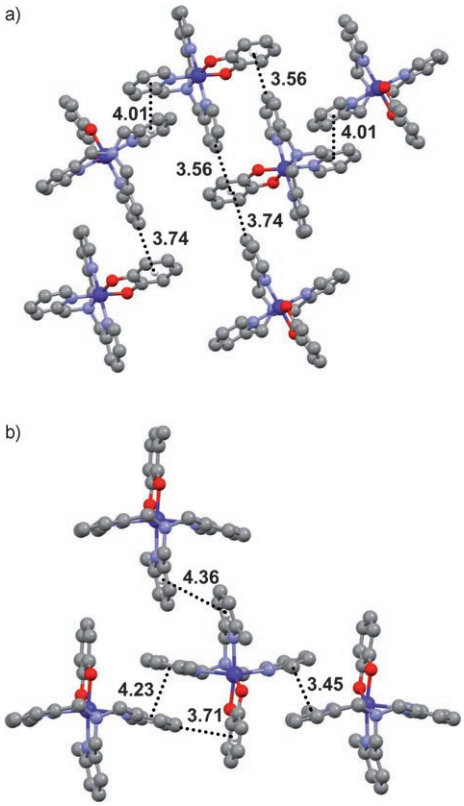

Figure 5. View of the relevant π–π and C–H···π interactions in the different derivatives. a) **1** (**2** and **3** show a closely related pattern), b) **4**.

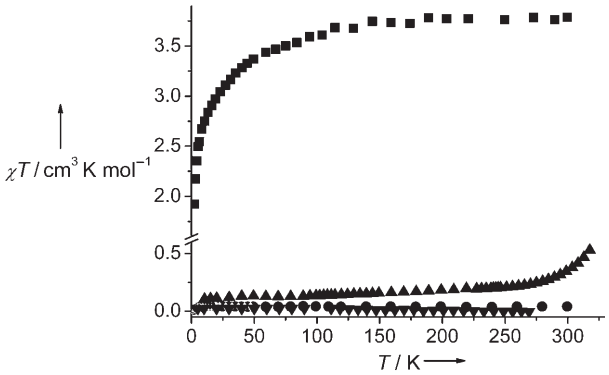

Figure 6. Plots of χT versus T for **1** (circles), **2** (inverse triangles), **3** (triangles), and **4** (squares).

this system, which leads to an increased bond length for the metal-ion coordination sphere, thus decreasing the ring slippage between adjacent pyridine units in one direction, and increasing it in the other direction.

Finally, it must be stressed that while crystals of **1** and **3** were obtained as ethanol-solvate derivatives, **2** and **4** were obtained from toluene (see the Experimental Section) and thus contain toluene molecules of crystallisation. This behaviour may lead to some differences in the expected interlayer interactions, which may be of relevance in determining the photomagnetic behaviour of the systems.

Magnetic properties: Solid-state magnetic measurements for polycrystalline samples of **1**–**4**, crystallized from solutions in ethanol, are reported in Figure 6. Both **1** and **2** are diamagnetic within the whole investigated temperature range (up to 300 K), thus clearly indicating a Co^{III}–Cat charge distribution, as expected on the basis of the molecular structure determined by X-ray studies. Conversely, the data of χT versus T for **3** indicate a Co^{III}–Cat charge distribution up to 280 K, but above this temperature a gradual increase in the paramagnetism of the sample is clearly observed, thus demonstrating the occurrence of an entropy-driven valence-tautomeric transition to the Co^{II}–SQ charge distribution. This behaviour is more clearly realised by studying the sample up to 320 K, at which point the χT value reaches 0.82 $cm^3 K mol^{-1}$. This value suggests that the transition temperature, defined as the temperature at which the two species are present in equimolar amounts, should be around 370 K, as estimated by a nonconclusive fitting of the curve of χT versus T by using the regular solution model.[51] Finally, the behaviour of χT versus T for **4** is clearly indicative of the Co^{II}–SQ charge distribution over the whole temperature range; indeed, the observed value of 3.75 $cm^3 K mol^{-1}$ at room temperature is completely compatible with the presence of an uncoupled distorted octahedral cobalt(II) ion with a largely unquenched orbital contribution ($\chi T = 3$–3.4 $cm^3 K mol^{-1}$) and a semiquinone radical. The decrease in the χT values observed on cooling should be attributed to cobalt(II) single ion effects, that is, to the depopulation of the higher multiples that arise from the splitting of the $^4T_{1g}$ orbital produced by the combined action of spin–orbit coupling and low-symmetry distortions.[52]

These results lead to the conclusions that in the solid state the Co^{II}–SQ species is favoured by increasing the number of methyl substituents on the ancillary ligand, whereas the Co^{III}–Cat species is favoured by low methyl substitution, as could also be inferred by the electrochemical data and electronic spectra of the samples in solution.

Photomagnetic properties: Irradiation of the ethanol solvates of **1**–**3** with light of different frequencies at low temperature results in the photoinduction of a small fraction (about 1–3 %) of Co^{II}–SQ species. The low conversion rate, which is a common feature of the photoinduced valence tautomerism in cobalt–dioxolene systems, might be attributed to different factors, namely, the strong opacity of the sample, which prevents the penetration of the light in the bulk, or the overlap of the transitions of the two different species. In the latter case, it is possible that these transitions result in the opposite interconversion, thus defining the photostationary state. A factor that can not be excluded is the possibility that the transformation occurs only at the surface of the sample as a consequence of the large variation in the molecular volume that accompanies this type of transition.

The corresponding thermal relaxations of the converted fraction at 9 K are shown in Figure 7. It is evident that the decay is very fast for **1** but much slower, and in comparable

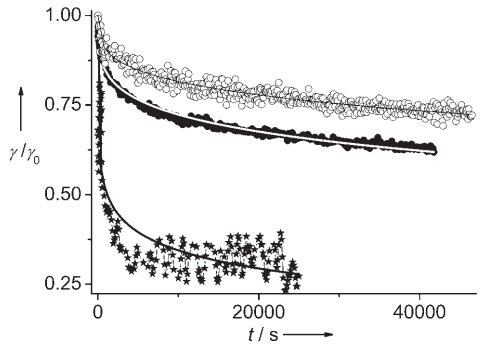

Figure 7. Relaxation kinetics of the photoinduced fraction of the ethanol solvates of **1** (stars), **2** (empty circles), and **3** (full circles) at 9 K. The converted fraction is normalized at 1 when $t=0$. The continuous lines are the best fits using the stretched exponential law with parameters reported in the text.

magnitude, for **2** and **3**, with the decay of latter being slightly faster. The experimental relaxation curves, normalized to the photoinduced fraction, were fitted to a first-order stretched exponential expression $\gamma_t/\gamma_0=\exp(\tau/t)^{\beta}$, where γ_t is the converted molar fraction of the metastable state at the time t, γ_0 is the photoinduced molar fraction at $t=0$, τ is the average relaxation time, and β is a parameter lying between 0 and 1 that accounts for a time-evolving distribution of activation energies. The best-fit curves were obtained for values of τ of approximately 1000 s, 1.9×10^6 s, and 4.5×10^5 s for **1**–**3**, respectively, with $\beta=0.3$. To check the effect of the solvent on the photomagnetic properties and to correlate the observed results with the X-ray structures of the compounds, we also irradiated the toluene derivative of **2**. The average relaxation time for the latter turned out to be about half of that for the ethanol solvate (8×10^5 s versus 1.9×10^6 s; see the Supporting Information). No definite photomagnetic effects (i.e., the occurrence of the reverse valence-tautomeric process Co^{II}–SQ→Co^{III}–Cat) were detected for **4**.

Discussion

We suggest that the observed trend in the properties of **1**–**4** is determined by the different zero-point energy changes $\Delta G°$ that characterise the valence tautomeric process in the different complexes. The $\Delta G°$ values at cryogenic temperatures were largely determined by the enthalpy changes associated with Equation (2) and by crystal-lattice energies. For this reason, the observed pattern of ΔG values in solution should be qualitatively indicative of the $\Delta G°$ values.

We note that the free-energy difference between the two isomers corresponds to the energy associated with the transition from the ground state to the first CT excited state if the two states are in vibrational and solvation equilibria. In principle, it should then be possible to evaluate its value from the energy associated with the first CT transition in the electronic spectrum. However, the optical transitions involve an excitation between a ground-donor level in the vibrational equilibrium and a nonequilibrium acceptor level; therefore, the difference in the solvation energy of the ground excited states and the reorganization energy of the excited state should also be considered.[42,53–58] As a consequence, we have used an empirical approach based on the electrochemical data to determine the ΔG values for valence-tautomeric equilibria involving **1**–**4**.

The free-energy changes estimated through this procedure well account for the room-temperature charge distribution observed in solution by the electronic spectra. Indeed, the ΔG values are positive for **1** and **2** but negative for **4** and, even if only weakly, **3**. These data are also in good agreement with the observations in the solid state (the magnetic properties and X-ray structures at 150 K), thus pointing to a Co^{III}–Cat distribution for **1** and **2** up to room temperature, whereas **3** undergoes an entropy-driven valence-tautomeric interconversion just above room temperature and **4** is characterised by the Co^{II}–SQ charge distribution.

If we further assume that the equilibria for the four derivatives are characterised by similar $T\Delta S$ values, the observed ΔG pattern should reflect that of the associated enthalpy variations. In particular, since temperature-dependent electrochemical studies concerning the $[Fe^{III}(L)Cat]/[Fe^{II}(L)SQ]$ interconversion (L = tetradentate macrocycle) suggested that the $T\Delta S$ quantity may be estimated to be on the order of 15 kJ mol^{-1} at 298 K,[42] we may assume that the **1**–**4** series is characterised by a similar constant value. On this basis, the calculated free-energy differences at 0 K (i.e., the enthalpy changes) will be $\Delta G=61$, 34, 6, and -25 kJ mol^{-1} (corresponding to 4900, 2700 , 500, and -2100 cm^{-1}, respectively). If these values hold also in the solid state, as the prediction of correct charge distribution at room temperature suggests, they should result in the observed relaxation rates k ($=\tau^{-1}$) varying in the order **1** > **2**(≈**4**) > **3**. This behaviour is in contrast to the experimental observations; indeed, while **1** shows the shortest lived photoinduced metastable state, the lifetime of the photoinduced state of **3** is almost an order of magnitude less than that of **2**. On the basis of the crystal structure description, one possible explanation for this discrepancy might be the strength of the intralayer interactions, which was shown to increase in the order **1** < **3** < **2** from X-ray structure analysis. This explanation would increase the 2D cooperativity of the photoinduced valence-tautomeric transition, thus justifying a corresponding increase in the lifetime of the photoinduced state. However, an active role of the solvents in the modulation of the interlayer interactions, and thus in an eventual variation in 3D cooperativity, can not be excluded, as seen by the different relaxation rates obtained for the two different solvates of **2**.

Experimental Section

Materials: All the reagents and solvents were obtained commercially and used as received, except dichloromethane and acetonitrile, which were dried over CaH_2. 6-Methyl-2-methylaminopyridine was prepared according to a previously reported procedure.[59]

Synthesis

Tris(2-pyridylmethyl)amine (tpa): This ligand was synthesised according to a reported procedure.[44] Pyridine-2-carboxyaldehyde (4.49 g, 42 mmol) was added to a stirred mixture of 2-aminomethylpyridine (2.16 g, 21 mmol) and sodium triacetoxyborohydride (12.48 g, 42 mmol) in dichloromethane (400 mL). The resulting reaction mixture was stirred for 18 h, after which a saturated aqueous solution of sodium hydrogencarbonate (200 mL) was added. The reaction mixture was stirred for 0.5 h and then extracted with ethyl acetate. The organic fraction was separated, dried over $MgSO_4$, and the solvent was removed under reduced pressure. The residue was extracted several times with pentane, and the solvent was removed to give tpa as light-yellow solid (5.42 g, 89%). Elemental analysis (%) calcd for $C_{18}H_{18}N_4$: C 74.46, H 6.24, N 19.30; found: C 74.61, H 5.97, N 19.42.

Bis(2-pyridylmethyl)(6-methyl-2-pyridylmethyl)amine (Metpa): This ligand was prepared by following the same procedure described above for tpa by replacing pyridine-2-carboxyaldehyde with 6-methylpyridine-2-carboxyaldehyde (5.17 g, 77%). Elemental analysis (%) calcd for $C_{19}H_{20}N_4$: C 74.97, H 6.62, N 18.41; found: C 74.76, H 6.23, N 18.12.

Bis(6-methyl-2-pyridylmethyl)(2-pyridylmethyl)amine (Me_2tpa): This ligand was prepared by following the same procedure described above for tpa by replacing 2-aminomethylpyridine with 6-methyl-2-aminomethylpyridine (5.31 g 83%). Elemental analysis (%) calcd for $C_{20}H_{22}N_4$: C 75.44, H 6.96, N 17.60; found: C 74.88, H 6.73, N 17.35.

Tris(6-methyl-2-pyridylmethyl)amine (Me_3tpa): This ligand was prepared by following the same procedure described above for tpa by replacing pyridine-2-carboxyaldehyde with 6-methyl-pyridine-2-carboxyaldehyde and 2-aminomethylpyridine with 6-methyl-2-aminomethylpyridine (5.73 g, 82%). Elemental analysis (%) calcd for $C_{21}H_{24}N_4$: C 75.87, H 7.28, N 16.85; found: C 75.67, H 7.01, N 16.46.

Synthesis of the [M(Me_ntpa)(DBdiox)]PF_6 (M=Co, Ni): Solutions of cobalt or nickel chloride (0.5 mmol) and the appropriate ligand (0.55 mmol) in methanol (30 mL) were mixed with a solution of the appropriate 3,5-di-*tert*-butylcatechol (0.5 mmol) and triethylamine (1.2–1.4 mmol) in methanol (30 mL) in an inert atmosphere. The metal(II)–(Me_ntpa)—catecholato complexes were oxidised with atmospheric dioxygen and the resulting products were precipitated by adding an aqueous solution of KPF_6. The cobalt complexes were recrystallised from ethanol or toluene. **1**·C_2H_5OH: elemental analysis (%) calcd for $C_{34}H_{44}CoF_6N_4O_3P$: C 53.69, H 5.83, N 7.37; found: C 53.51, H 5.92, N 7.15; electronic spectra: absorption maxima (ε in parentheses): 13650 (220), 23200 (460), 28500 (sh) cm^{-1}. **2**·C_2H_5OH: elemental analysis (%) calcd for $C_{35}H_{46}CoF_6N_4O_3P$: C 54.28, H 5.99, N 7.23; found: C 53.97, H 5.80, N 7.07; electronic spectra: absorption maxima (ε in parentheses): 12150 (230), 21530 (330), 27000 (sh) cm^{-1}. [Co(Me_2tpa)(dbcat)]PF_6 (**3**·C_2H_5OH): elemental analysis (%) calcd for $C_{36}H_{48}CoF_6N_4O_3P$: C 54.80, H 6.14, N 7.11; found: C 54.61, H 5.95, N 6.97; electronic spectra: absorption maxima (ε in parentheses): 12500 (400), 15150 (720), 17500 (890), 19000 (750), 23350 (1070) cm^{-1}. **2**·C_7H_8: elemental analysis (%) calcd for $C_{40}H_{48}CoF_6N_4O_2P$: C 58.54, H 5.89, N 6.83; found: C 58.35, H 6.05, N 6.68. **4**·C_7H_8: elemental analysis (%) calcd for $C_{42}H_{52}CoF_6N_4O_2P$: C 59.53, H 6.17, N 6.60; found: C 59.71, H 6.14, N 6.42; electronic spectra: absorption maxima (ε in parentheses): 12500 (420), 15150 (790), 17500 (870), 18900 (790), 23350 (1200) cm^{-1}. [Ni(tpa)(dbsq)]PF_6·H_2O: elemental analysis (%) calcd for $C_{32}H_{40}NiF_6N_4O_3P$: C 52.48, H 5.50, N 7.65; found: C 52.88, H 5.63, N 7.40. [Ni(Metpa)(dbsq)]PF_6·H_2O: elemental analysis (%) calcd for $C_{33}H_{42}NiF_6N_4O_3P$: C 53.10, H 5.67, N 7.51; found: C 52.78, H 5.68, N 7.35. [Ni(Me_2tpa)(dbsq)]PF_6·H_2O: elemental analysis (%) calcd for $C_{34}H_{44}NiF_6N_4O_3P$: C 53.70, H 5.83, N 7.37; found: C 53.21, H 5.64, N 7.42. [Ni(Me_3tpa)(dbsq)]PF_6·H_2O: elemental analysis (%) calcd for $C_{35}H_{46}NiF_6N_4O_3P$: C 54.28, H 5.99, N 7.23; found: C 53.80, H 6.15, N 7.06.

Electronic spectra: Visible absorption spectra of the four derivatives were recorded in solution with CH_2Cl_2 in the visible region with a Perkin-Elmer Lambda 20 Bio instrument.

Electrochemistry: All the electrochemical measurements were performed with an AUTOLAB PGSTAT 10 digital potentiostat/galvanostat, controlled by the GPES 4.9004 software (Eco Chemie BV, Utrecht, The Netherlands). The experiments were performed at 25°C in acetonitrile with 0.1 M NBu_4PF_6 added as the supporting electrolyte and a Pt wire as the working electrode. An acetonitrile-based reference electrode was constructed by dropping an Ag/AgCl wire in a vial containing acetonitrile with 0.1 M NBu_4Cl added. A salt bridge guaranteed the contact between the obtained pseudo-reference electrode and the solution to be tested. The analyzed potential range was $-1.0/+1.75$ V (versus the pseudoreference electrode) at a scan rate of 50 $mV\,s^{-1}$.

Magnetic and photomagnetic properties: The magnetic properties of polycrystalline samples of **1**–**4** were measured at 2–320 K with applied magnetic fields of 1 Tesla using a Cryogenic S600 SQUID magnetometer. The data were corrected for the magnetism of the sample holder, which was determined separately in the same temperature range and field, and the underlying diamagnetism of each sample was estimated from the Pascal constants. The photomagnetic characterisation of the samples was performed with the irradiation of thin pellets (2–3 mg) obtained from polycrystalline powder. The S600 Cryogenic SQUID Magnetometer has been equipped with an optical fibre and a specifically designed sample holder. The samples were irradiated using CW laser diodes with light with an output power of up to 10 $mW\,cm^{-2}$. Earlier calibration of the setup was accomplished to remove any stray contributions as a result of the arrangement and any warming effect on the sample.[39] Several frequencies, all belonging to the visible/NIR region were used to trigger the photoconversion since the absorption spectra of the compounds showed several quite broad bands in all the visible range. The variation of the magnetisation of the sample was, thus, followed as a function of the irradiation time at a constant temperature of 9 K. The more efficient processes were obtained by using by light of $\lambda = 405$, 650, and 904 nm for **1**—**3**, respectively. The percentage of photoconversion was evaluated according to $(\chi T(t=0)-\chi T_{OFF})/(\chi T_{Co^{II}\text{-}SQ}-\chi T_{OFF})$ where $\chi T(t=0)$ is the photostationary value obtained after irradiation, χT_{OFF} is the value for each compound at 9 K and $\chi T_{Co^{II}\text{-}SQ}$ is the value relative to the Co^{II}–SQ species at the same temperature. Assuming that the different systems were subjected to the same ligand field, the latter value was directly obtained by the measure of sample **4** (2.44 $cm^3\,K\,mol^{-1}$). The relaxation kinetics were recorded by switching off the laser light as soon as the photostationary limit was achieved. The photostationary limit was reached for all the compounds after 10 h of continuous irradiation at 9 K, thus giving Co^{II}–SQ conversion as <1, 1, and 3% for **1**–**3**, respectively. Subsequent tests performed by varying the output laser power from 1 to 10 $mW\,cm^{-2}$ showed that no effect of the increased intensity was observed on the conversion percentage. For all the measurements, the reversibility was tested by increasing the temperature up to 80 K to allow full relaxation of the photoinduced metastable fraction and afterwards further thermalizing at 9 K. This test can be considered analogous to the T_{LIESST} measurement.[37]

X-ray crystallography: X-ray data collection for **1**–**4** was performed on an Oxford Instrument XCALIBUR-3 kappa-4 circle diffractometer equipped with the Sapphire 3 CCD area detector and using graphite-monochromated $Mo_{K\alpha}$ radiation from the Enhance high-brilliance sealed tube. The diffraction data were collected at 150 K using an Oxford Cryostream liquid-nitrogen cooling system. Details of the unit cell and the refinement results are reported in Table 1; selected parameters or ranges are given in Table 2; the structures were solved by direct methods using SIR97[60] and refined using the full-matrix least-squares method on F^2 with the SHELXL-97 package.[61]

CCDC-629868, -655675, -638171, and -629869 for **1**–**4**, respectively, contain the supplementary crystallographic data for this paper. These data can be obtained free of charge from the Cambridge Crystallographic Data Centre via www.ccdc.cam.ac.uk/data_request/cif.

Acknowledgements

The authors acknowledge the financial support of the EU through NoE MagMANet (contract NE: NMP3-CT-2005–515767) and the Italian MIUR through FIRB project (FIRB 2003: Sintesi e caratterizzazione di materiali molecolari e polimerici con proprietà optoelettroniche e fotoniche).

[1] *Photochemistry and Radiation Chemistry: Complementary Methods for the Study of Electron Transfer* (Eds: J. F. Wishart, D. Nocera), ACS Advances in Chemistry Series 254, American Chemical Society, Washington DC, **1998**.
[2] V. Balzani, A. Credi, F. Scandola, *Supramolecular Photochemistry and Photophysics: Energy Conversion and Information-Processing Devices Based on Transition-Metal Complexes, NATO ASI Ser. Ser. C.: Math. Phys. Sci.* **1994**, *448*, 1.
[3] K. Kalyanasundaram, M. Grätzel, *Coord. Chem. Rev.* **1998**, *177*, 347.
[4] M. Marchi, J. N. Gehlen, D. Chandler, *J. Am. Chem. Soc.* **1993**, *115*, 4178.
[5] J. S. Connolly, J. R. Bolton, *Photoinduced Electron Transfer* (Eds: M. A. Fox, M. Channon), Elsevier, Amsterdam, Part D, p. 303, **1988**.
[6] B. O'Regan, M. Grätzel, *Nature* **1991**, *353*, 738.
[7] J. K. McCusker, *Acc. Chem. Res.* **2003**, *36*, 876.
[8] R. Argazzi, N. H. Murakami Yha, H. Zabri, F. Odobel, C. A. Bignozzi, *Coord. Chem. Rev.* **2004**, *248*, 1299.
[9] E. A. Juban, A. L. Smeigh, J. E. Monat, J. K. McCusker, *Coord. Chem. Rev.* **2006**, *250*, 1783.
[10] R. A. Marcus, N. Sutin, *Biochim. Biophys. Acta* **1985**, *811*, 265.
[11] O. Sato, J. Tao, Y.-Z. Zhang, *Angew. Chem.* **2007**, *119*, 2200; *Angew. Chem. Int. Ed.* **2007**, *46*, 2152.
[12] O. Sato, A. Cui, R. Matsuda, J. Tao, S. Hayami, *Acc. Chem. Res.* **2007**, *40*, 361–369.
[13] A. Dei, D. Gatteschi, C. Sangregorio, L. Sorace, *Acc. Chem. Res.* **2004**, *37*, 827.
[14] O. Sato, *J. Photochem. Photobiol. C* **2004**, *5*, 203.
[15] P. Gütlich, Y. Garcia, T. Woike, *Coord. Chem. Rev.* **2001**, *219–221*, 839.
[16] C. Brady, J. J. McGarvey, J. K. McCusker, H. Toflund, D. N. Hendrickson, *Top. Curr. Chem.* **2004**, *235*, 1.
[17] A. Hauser, *Top. Curr. Chem.* **2004**, *235*, 155.
[18] P. Gütlich, Y. Garcia, H. A. Goodwin, *Chem. Soc. Rev.* **2000**, *29*, 419.
[19] J. A. Real, A. B. Gaspar, M. C. Munoz, *Dalton Trans.* **2005**, 2062.
[20] A. Beni, C. Carbonera, A. Dei, J.-F. Létard, R. Righini, C. Sangregorio, L. Sorace, *J. Braz. Chem. Soc.* **2006**, *17*, 1522.
[21] E. Evangelio, D. Ruiz-Molina, *Eur. J. Inorg. Chem.* **2005**, 2957.
[22] D. N. Hendrickson, C. G. Pierpont, *Top. Curr. Chem.* **2004**, *234*, 63.
[23] C. G. Pierpont, *Coord. Chem. Rev.* **2001**, *216–217*, 99.
[24] D. A. Shultz in *Magnetism – From Molecules to Materials* (Eds: J. S. Miller, M. Drillon), Wiley-VCH, Weinheim, **2001**.
[25] P. Gütlich, A. Dei, *Angew. Chem.* **1997**, *109*, 2852; *Angew. Chem. Int. Ed. Engl.* **1997**, *36*, 2734.
[26] D. M. Adams, A. Dei, A. L. Rheingold, D. N. Hendrickson, *J. Am. Chem. Soc.* **1993**, *115*, 8221.
[27] O.-S. Jung, C. G. Pierpont, *Inorg. Chem.* **1994**, *33*, 2227.
[28] J. Tao, H. Maruyama, O. Sato, *J. Am. Chem. Soc.* **2006**, *128*, 1790.
[29] D. M. Adams, D. N. Hendrickson, *J. Am. Chem. Soc.* **1996**, *118*, 11515.
[30] A. Caneschi, A. Cornia, A. Dei, *Inorg. Chem.* **1998**, *37*, 3419.
[31] D. Ruiz-Molina, J. Veciana, K. Wurst, D. N. Hendrickson, C. Rovira, *Inorg. Chem.* **2000**, *39*, 617.
[32] A. Caneschi, A. Dei, F. Fabrizi de Biani, P. Gütlich, V. Ksenofontov, G. Levchenko, A. Hoefer, F. Renz, *Chem. Eur. J.* **2001**, *7*, 3926.
[33] O. Sato, S. Hayami, Z.-Z. Gu, K. Seki, R. Nakjima, A. Fujishima, *Chem. Lett.* **2001**, 874.
[34] O. Sato, S. Hayami, Z.-Z. Gu, K. Takahashi, R. Nakajima, A. Fujishima, *Chem. Phys. Lett.* **2002**, *355*, 169.
[35] F. V. R. Neuwahl, R. Righini, A. Dei, *Chem. Phys. Lett.* **2002**, *352*, 408.
[36] C. Carbonera, A. Dei, J.-F. Létard, C. Sangregorio, L. Sorace, *Angew. Chem.* **2004**, *116*, 3198; *Angew. Chem. Int. Ed.* **2004**, *43*, 3136.
[37] C. Carbonera, A. Dei, C. Sangregorio, J.-F. Létard, *Chem. Phys. Lett.* **2004**, *396*, 198.
[38] J. Tao, H. Maruyama, O. Sato, *J. Am. Chem. Soc.* **2006**, *128*, 1790.
[39] A. Beni, A. Dei, D. A. Shultz, L. Sorace, *Chem. Phys. Lett.* **2006**, *428*, 400.
[40] A. Hauser, C. Enachescu, M. L. Daku, A. Vargas, N. Amstutz, *Coord. Chem. Rev.* **2006**, *250*, 1642.
[41] E. Buhks, G. Navon, M. Bixon, J. Jortner, *J. Am. Chem. Soc.* **1980**, *102*, 2918.
[42] A. Dei, *Inorg. Chem.* **1993**, *32*, 5730.
[43] A. Bencini, A. Caneschi, C. Carbonera, A. Dei, D. Gatteschi, R. Righini, C. Sangregorio, J. Van Slageren, *J. Mol. Struct.* **2003**, *656*, 141.
[44] H. Nagao, N. Komeda, M. Mukaida, M. Suzuki, K. Tanaka, *Inorg. Chem.* **1996**, *35*, 6809.
[45] A. Beni, A. Dei, M. Rizzitano, L. Sorace, *Chem. Commun.* **2007**, 2160.
[46] G. J. P. Britovsek, J. England, A. J. P. White, *Inorg. Chem.* **2005**, *44*, 8125.
[47] Benelli, A. Dei, D. Gatteschi, L. Pardi, *Inorg. Chim. Acta* **1989**, 163, 99.
[48] A. B. P. Lever, *Inorganic Electronic Spectroscopy*, Elsevier, Amsterdam, **1984**.
[49] A. Caneschi, A. Dei, D. Gatteschi, V. Tangoulis, *Inorg. Chem.* **2002**, *41*, 3508.
[50] C. Janiak, *J. Chem. Soc. Dalton Trans.* **2000**, 3885–3896.
[51] O. Kahn, *Molecular Magnetism*, Wiley-VCH, Weinheim, **1993**.
[52] A. Bencini, A. Beni, F. Costantino, A. Dei, D. Gatteschi, L. Sorace, *Dalton Trans.* **2006**, 722.
[53] R. A. Marcus, *J. Chem. Phys.* **1965**, *43*, 1261.
[54] A. B. P. Lever, S. R. Pickens, P. C. Minor, S. Licoccia, B. S. Ramaswami, K. Magnell, *J. Am. Chem. Soc.* **1981**, *103*, 6800.
[55] A. B. P. Lever, *Inorg. Chem.* **1990**, *29*, 1271.
[56] H. Masui, A. B. P. Lever, E. S. Dodsworth, *Inorg. Chem.* **1993**, *32*, 258.
[57] E. H. Kober, B. P. Sullivan, T. J. Meyer, *Inorg. Chem.* **1984**, *23*, 2098.
[58] E. H. Kober, J. V. Caspar, B. P. Sullivan, T. J. Meyer, *Inorg. Chem.* **1988**, *27*, 4587.
[59] O. Fuentes, W. W. Paudler, *J. Org. Chem.* **1975**, *40*, 1210.
[60] A. Altomare, M. C. Burla, M. Camalli, G. L. Cascarano, C. Giacovazzo, A. Guagliardi, A. G. G. Moliterni, G. Polidori and R. Spagna, *J. Appl. Crystallogr.* **1999**, *32*, 115.
[61] G. M. Sheldrick, SHELXL-97, University of Göttingen, Germany, **1997**.

Received: July 27, 2007
Published online: December 3, 2007

